ASM Sc. J., 17, 2022

https://doi.org/10.32802/asmscj.2022.944

Study on Photocatalytic Efficiency of Hybrid Titanium Dioxide Nanowires/Reduced Graphene Oxide (TiO_2NWs/RGO) for Degradation of Methyl Orange Dye

Basirah Mohd Azam[1], Mohd Hasmizam Razali[1,2*] and Muhammad Amir Fikri Md Fauzi[1]

[1]*Faculty of Science and Marine Environment, Universiti Malaysia Terengganu, 21030 Kuala Nerus, Terengganu, Malaysia*

[2]*Advanced Nanomaterials Research Group, Faculty of Science and Marine Environment, Universiti Malaysia Terengganu, 21030 Kuala Nerus, Terengganu, Malaysia*

The major concern of this research is to improve photocatalytic efficiency by implementation of hybrid TiO_2NWs/RGO for dye degradation. The TiO_2NWs/RGO was prepared using fabrication method. Titanium (IV) oxide powder and graphite were used as precursors to synthesis of TiO_2NWs and RGO, respectively. Physical and chemical properties of the photocatalyst was investigated by Fourier Transform Infrared (FTIR), X-Ray Diffraction (XRD), Scanning Electron Microscopy (SEM), Adsorption-desorption nitrogen analysis and their photocatalytic efficiency was studied for methyl orange (MO) degradation. The hybrid almost achieved 100% of MO degradation within 210 minutes and shows the highest photocatalytic activity. Furthermore, It was fixed to the Langmuir–Hinshelwood model and the degradation of MO dye by each sample obeys first-order reaction kinetics that it shows a good performance of photodegradation rate of dyes by heterogenous catalyst. This is due the 1D/2D heterostructures of TiO_2NWs/RGO hybrid that has a large surface area, unique optical properties, flexible structure and excellent mobility of charge carriers.

Keywords: nanocomposites; photocatalyst; graphene; degradation; dye

I. INTRODUCTION

The industry is using various chemicals including dye in processes of textile manufacture has created a huge pollution problem as it is one of the most chemically intensive industries on earth, and the no. 2 polluter of clean water after agriculture (Khan *et al.,* 2019). Dyes can be converted to the carcinogenic compounds or toxic. Seriously, it affects the aesthetic quality and transparency of water bodies such as rivers, lakes and others, leading to damage to the aquatic environment (Kamalan *et al.,* 2018). There are many process of water treatment including traditional chemical, electrochemical and biological treatment, but this approach is limited due to low degradation performance, chemical consumption and the generation of secondary pollution (Abdel-Messih *et al.,* 2013). To find a suitable process to remove these harmful pollutants, the photocatalysis seems to be a very economical and efficient approach to this issue (Makal & Das, 2019). An organic compound from dye can decompose into water (H_2O) and carbon dioxide (CO_2) in photodegradation of materials, which involve the generation of hydroxyl radicals (OH) that is powerful, non-selective chemical oxidant and acts very rapidly with most of the organic compounds (Pandey *et al.,* 2015) in sufficient quantity to effect water purification. Recent research has shown that the Titanium Dioxide (TiO_2) materials synthesised by hydrothermal method can be used as photocatalyst to degrade a variety of organic contaminants (Zhao *et. al.,* 2010; Santhi *et al.,* 2019)

*Corresponding author's e-mail: mdhasmizam@umt.edu.my

because of their being able to control particle size and nanostructure at low temperatures as well as being a cost-effective synthesis method accomplished of large-scale production (Asiah *et al.,* 2013). Despite all the amazing properties of TiO_2 such as photostability, intrinsic electronic and surface properties, non-toxicity, cost-effectiveness, and environmental friendliness (Kumar & Devi *et. al.,* 2011; Schneider *et al.,* 2014), it suffers from the small surface area, large band gap which inhabits about 4% of the sunlight and cause separation possibility of photo-induced electron-hole pairs in photocatalysts is low (Najafi *et al.,* 2017). New ways to produce more effective photocatalysts like combining semiconductors, noble metal doping, and loading that recently gotten a lot of attention from many researchers. In addition, TiO_2-carbon composites can also show good photocatalytic activity under UV light (Liu & Zeng, 2008). As one of the most popular two-dimensional (2D) graphitic carbon materials, graphene possesses excellent physical and chemical properties (Zhao *et al.,* 2014). Graphene and graphene derivatives are being used because of their special properties of high optical transparency, high electrical conductivity, and charge transport as well as have a large surface area (Gao *et. al.,* 2012; Li *et al.,* 2018). Hybrid catalysts containing graphene oxide (GO) or reduced graphene oxide (RGO) seem to have greater absorptivity (Xie *et al.,* 2015), rapid bonding of organic molecules to the surface active sites with functional groups (Wei *et al.,* 2019), rapid charge separation, increased photocatalytic activity, and high conductivity with a large surface area (Akyuz *et al.,* 2016). For instance, RGO shows a specific narrow band gap energy and visible light response eliminates deficiencies in degradation of dye (Gonçalves *et. al.,* 2019; Singh *et al.,* 2020). RGO also was used as supports to remove the cationic impurities such as cationic dyes and heavy metal cations (Putri *et al.,* 2016). In addition, The Langmuir–Hinshelwood Kinetic model was used to investigate the kinetics of photocatalyst in dye degradation (Bhatia & Verma, 2017). Because it allows one to assess photocatalytic activity irrespective of the earlier adsorption duration in the dark and the concentration of solute left in the solution, the apparent rate constant (k) has been chosen as the basic kinetic parameter for the various photocatalysts. Therefore TiO_2 nanowires (TiO_2NWs) was synthesised and coupled with Reduced Graphene Oxide (RGO) to produce TiO_2NWs/RGO hybrid photocatalyst for degradation of methyl orange dye.

II. MATERIALS AND METHOD

All chemicals and solvents were purchased from Merck (Germany). The apparatus and glassware ware used are beakers (50ml, 100ml, 250ml and 500ml). Measuring cylinder (10ml, 50ml, 100ml), magnetic stirrer, hotplate stirrer, spatula, petri dishes, glass rod, pH paper, filter paper and 200 ml teflon autoclave reactor. Volumetric flask (1L), 10ml syringe and 0.5μm filter membrane of syringe, buchner funnel, filter flask, thermometer and crucible

A. Synthesis of Titanium Dioxide Nanowires (TiO_2NWs)

An amount 1g of TiO_2 was added to aqueous solution of 10M NaOH (100 ml) and the solution was stirred with the magnetic stirrer for 30 minutes to form homogeneous suspension and the resulting suspension solution was transferred into 80 ml Teflon-lined autoclave reactor for hydrothermal treatment at 160˚C for 10 hours in the furnace. When the reaction is complete, the white precipitate obtained was washed with deionised water followed by 0.1M HCl. The solution was filtered and washed with deionised water and ethanol, respectively to remove residual Na^+. Then, the white precipitate was dried at 40˚C for 24 hours in an oven. Lastly, the synthesised of TiO_2 was anneal at temperatures 500˚C for 2 hours to form TiO_2 nanowires structure.

B. Synthesis of Reduced Graphene Oxide (RGO)

RGO was prepared from the source of graphite and using modified Hummers method that is usually used to generate GO due to the more stable nature in order to create more harmless and non-toxic including the addition of sodium nitrate, rather than the use of nitric acid as a solvent, to form nitric acid in the original site, and the use of potassium permanganate ($KMnO_4$) as an oxidiser instead of potassium chloride ($KClO_3$), which produces toxic chlorine dioxide gas (Smith *et al.,* 2019). In a typical synthesis, 3 g of graphite powder and 1.5 g of $NaNO_3$ was poured into 23 ml of H_2SO_4 under rapid stirring to exfoliate the graphite flakes. After 30 minutes, 4 g of $KMnO_4$ was added into the reaction mixture slowly (maintain the temperature under 10 °C to avoid vigorous stirring) and the colour of the mixture turned purple-green. Next, the mixture solution was transferred into water bath and diluted with 46 ml of deionised water causing brown vapour evolution, resulting from the oxidation of $KMnO_4$ and the temperature was raised up to 98 °C. The mixture solution was diluted again with 140 ml of deionised water and the reaction was ended by addition 10 ml of H_2O_2 to eliminate residual $KMnO_4$ (the brown suspension changed to yellow colour). Further, the mixture solution was washed with 5% of HCl and repeated centrifuging with deionised water to completely remove residual H_2SO_4. To get in powder form, the synthesised product was dried in oven at 50 °C overnight. Dark brown precipitate as a GO is obtained and then put into the furnace at 500 °C for 2 hours to completely graphene oxide reduced.

C. Fabrication of TiO_2NWs/RGO Nanocomposites

1g of TiO_2NWs was added in 50 ml deionised water and put into ultrasonic for 30 minutes so that the solution was dispersed well. Next, the solution drop-wise into 1g of RGO nanosheets which dispersed in 100 ml deionised water. Then, the mixture solution mixed in ultrasonic for 3 hours. The obtained precipitate was centrifuged at 4000rpm (30 minutes). Finally, the precipitates were washed with deionised water several times and dried at 50 ˚C for 12 hours to remove residual H2O and get TiO_2NWs/RGO in powder form.

D. Sample Characterisation

FTIR spectra were conducted on Niconet 5700 FTIR spectrometer with the sample was dispersed in potassium bromide (KBr). The analysis was done from 400 – 4000 cm^{-1} wavenumber. X-ray diffraction (XRD) was utilised to study the crystal structure and XRD patterns were acquired on Bruker D8 Advance X-ray diffractometer (Bruker AXS, German) at a scanning speed of 0.2◦ s^{-1} from 10 to 90° of 2θ. The surface morphology of catalyst was determined using scanning electron microscopy (SEM) JEOL JSM 6360LA at the operational voltage of 10 kV. N2 adsorption-desorption isotherms were recorded using Micromeritics TriStar II, at −196.2 °C. Prior to this characterisation, samples were degassed at 120 °C for 2 h with nitrogen purging. Surface area, pore size and volume were determined using BET method. UV–Vis absorption spectra were analysed using a UV–Vis spectrophotometer (UV-2550, Shimadzu, Japan).

E. Photocatalytic Activity

An amount of catalyst was dissolved into 100ml of methyl orange solution (20ppm). Photocatalytic degradation was carried out in dark for 30 minutes to attain adsorption/ desorption equilibrium between dye and photocatalyst. Next, the solution (10ml) of initial concentration (Co) was taken out and then the solution continuously stirred was exposed to UV light. UV light irradiation was provided by two 15 W of UV-B lamps with a fixed distance of 50cm between samples and lamp. To determine the degradation of dye, samples were filter by using 0.5 μm filter membrane after regular intervals (30 min) during the reaction. The progress of MO dye degradation was monitor by considering the change in absorption peaks at 300nm to 600nm range in UV-Vis spectra. The photo-degradation efficiency (η) was calculated using Equation (1):

$$\text{Percentage degradation (\%)} = (A0 - At / A0) \times 100 \qquad (1)$$

Where *A*0 and *At* are the initial photocatalytic activity and the after photocatalytic activity various intervals of time (*t*), respectively.

III. RESULT AND DISCUSSION

The prepared photocatalyst samples were characterised using various techniques in order to study their physical and chemical properties. The photocatalytic activity was evaluated for degradation of methyl orange (MO) under dark and ultra-violet (UV) irradiation. The last part elaborates result and finding on kinetic studies that contribute to the good performance of photocatalyst.

A. Functional Group Analysis

The FTIR spectra of TiO_2NWs, RGO and TiO_2NWs/RGO hybrid photocatalyst samples were shown in Figure 1. Water (H_2O) molecules were present on the pure RGO and TiO_2NWs/RGO hybrid surfaces attributing to the existence of a broad peak around 3500-3400 cm^{-1}, which is assigned to O-H stretching mode of H_2O. Pure TiO_2NWs sample free from a water molecule and other contamination as an only single broad band was observed below 1000 cm^{-1} with maximum intensity at 498 cm^{-1} due to the metal and oxygen bond of O-Ti-O stretching (Makal & Das, 2019). For pure RGO sample Figure 1(ii), a peak around 1600 cm^{-1} was observed with low-intensity corresponding to the C=C aromatic of RGO molecule structure. On top of that, C-O stretching mode within 1250-1050 cm^{-1} suggesting the formation of RGO (Maruthamani *et al.,* 2015). The Peak at 1719 cm^{-1} corresponds to the carbonyl group (C=O) of carboxylic acid located at the surfaces of RGO nanosheets, indicating deoxidation of graphene oxide as during RGO synthesis (Bashiri *et al.,* 2020). The stretching band corresponds to C-OH and C-O symmetric stretching respectively at 1385 cm^{-1} and 1049 cm^{-1} (Khan *et al.,* 2019). Complete GO reduction was accomplished because no apparent peaks could be detected, indicating that all functional groups of carbon-oxygen existed, but their characteristic peaks are only very small. C=C stretching mode shifted slightly to a higher wavelength number 1616 cm^{-1}, probably due to the interaction of TiO_2NWs with RGO. While the peak belongs to Ti-O-Ti vibration is remained almost similar with the pure TiO_2 sample. In addition, the high absorption bands measured in the range 400–1000 cm^{-1} indicated the existence of Ti–O–C and Ti–O–Ti bonds in the samples representing the chemical bonding between the TiO2 surface hydroxyl groups and the graphene oxide functional group (Nguyen-Phan *et al.,* 2011).

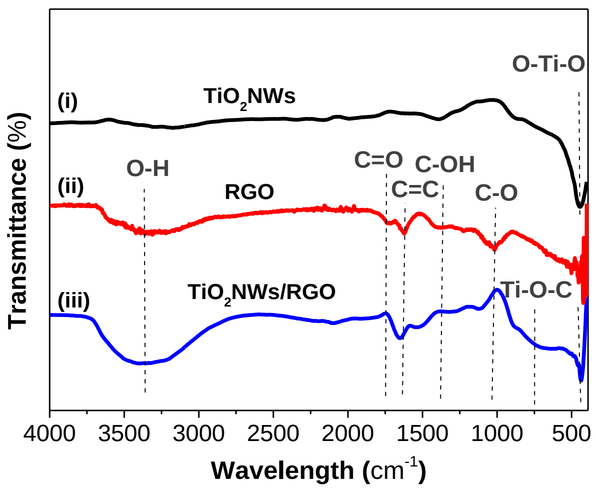

Figure 1. FTIR spectra of TiO_2NWs, RGO and TiO_2NWs/RGO

B. Crystal Structure and Crystallinity

Figure 2(i) shows the XRD pattern of TiO2NWs containing the peaks at 25.3, 37.8, 48.0, 53.9, 55.1, 62.7, 68.8, 70.3, and 75.0° can be indexed to (101), (004), (200), (105), (211), (204), (116), (220) and (215) tetragonal crystal planes of anatase TiO_2, as reported by other researchers previously (AlShammari *et al.,* 2020). Interestingly, no peaks assigned to the rutile and brookite phase were observed even though the sample had been calcined at 500°C during the preparation of TiO_2NWs. Anatase is most stable at low particle sizes (< 22 nm), while rutile phase is more stable in its bulk form. Because of its stability in the nanometer range, anatase is considered more suitable for catalytic applications (Barnard & Curtiss, 2005). Anatase phase has a stronger photocatalytic property due to the higher electron mobility in the anatase crystal structure and stable at high temperature compared to rutile and brookite metastable at high temperature (Marien *et. al.,* 2016; Hatefi *et al.,* 2021). The structure modification of anatase TiO_2 is used to decrease electron-hole recombination due to its low electron mobility, oxygen vacancy defects in surface TiO_2, and poor structural stability against UV light (Shymanovska *et al.,* 2021). Anatase has an indirect band gap while rutile and brookite have direct band gaps. The indirect band gap helps in delaying the recombination of photoexcited electron–hole pairs (Piler *et al.,* 2020). Also, the photogenerated charge carriers or excitons in anatase can easily diffuse to the surface to take part in photoreduction and photooxidation reactions as they have the lightest average effective mass when compared to rutile and brookite (Piler *et al.,* 2020).

The characteristic diffraction of TiO_2NWs/RGO in Figure 2(iii) at approximately 25.4°, 40°, and 49.3° are corresponding to the (101), (004), and (200) plane and all the diffraction peak can be indexed to anatase TiO2 phase structured (JCPDS: No.71–1166), which indicate the existence of TiO2 in the targeted hybrid samples. The strong (101) plane reflections of the TiO2NWs also masked the weak and broad characteristic peak of RGO at 2θ ~ 25° (Maruthamani *et al.,* 2015). On top of that in Figure 2(iii), it can be seen that the intensity of the TiO_2 anatase peaks decreases after modification with RGO and pure RGO shows a broad peak that could be easily overlapped with the anatase peak when the amount of graphene in the prepared sample is relatively low, suggesting that homogeneous mixture of TiO_2NWs and RGO in nanocomposite materials was obtained.

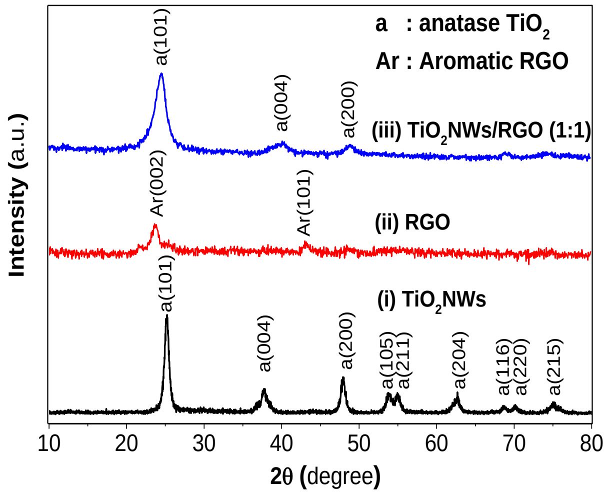

Figure 2. XRD patterns for TiO2NWs, RGO and TiO2NWs/RGO

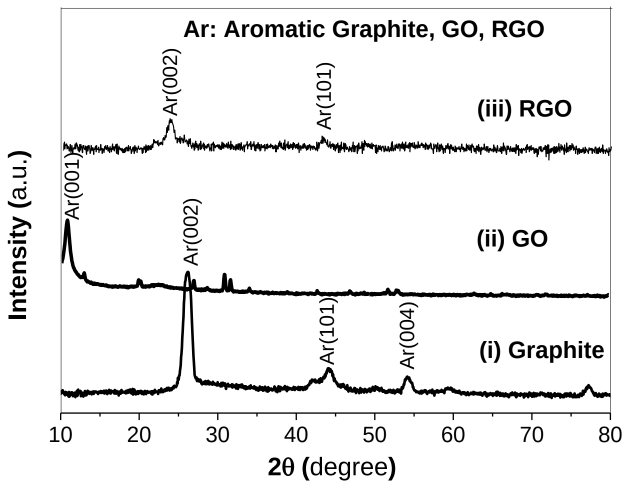

Figure 3. XRD patterns for Graphite, GO and RGO

RGO was formed from the source of graphite, a sharp peak was observed at 26.5˚ assigned to (002) together with the extra peaks at 45˚ and 55˚ attributed to the (101) and (004) planes of aromatic graphite in Figure 3(i), respectively. In contrast Figure 3(ii), the peaks of (002) shifted to a lower 2θ value from 26.5˚ to 11.8˚ for graphene oxide (GO) sample suggesting that the oxidation of graphite had occurred. Interestingly, it can be observed that the sharp peak at 11.8° which is assigned to (002) planes of aromatic GO is disappeared and shifted with low intensity when the GO has been converted into RGO. The reformation of the peak at 2θ = 25.7° confirmed the production of RGO attributed to the restoration of C-C bonding resulted from the reduced graphene oxide sheets in Figure 3(iii) (Ikram *et al.,* 2020).

C. Surface Morphological Analysis

SEM analysis was carried out to investigate the surface morphology of TiO_2NWs/RGO. The SEM image of the TiO_2NWs/RGO hybrid in Figure 4 displayed that TiO_2NWs around 20-30 nm in size are unevenly immobilised on the RGO layers (two-dimensional structure interlinking with wrinkles on the edge). In addition, the SEM image of the TiO_2NWs/RGO (Figure 4) demonstrated the presence of 0.35 nm interlayer spacing coincides with the (101) lattices spacing of anatase TiO_2 (Geng *et. al.,* 2019; Boruah *et al.,* 2019), and there are abundant oxygen holes on the anatase TiO_2 (101) crystal surface, which can be used as electron adsorption centres in the photocatalytic process, thereby efficiently promoting the photocatalytic reaction of methyl orange dye.

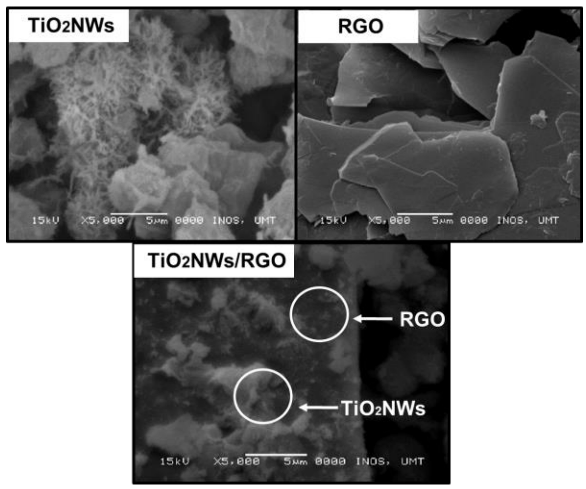

Figure 4. SEM image for TiO_2NWs, RGO and TiO_2NWs/RGO

D. Surface Textural Analysis

Surface texture study the Brunauer-Emmett-Teller (BET) theory is well-known as a valuable method for studying the surface texture properties of solid powders. The typical N_2 adsorption-desorption isotherms of individual and hybrid samples are illustrated in Figure 5. As shown, adsorption and desorption divisions are close for each isotherm, representing the formation of uniform pores in the sample

(Norouzi *et al.,* 2021). The specific surface area and porosity influence the efficiency of the photocatalyst. The S_{BET} has shown that the surface areas of pure TiO_2 are low only 29.97 m^2/g attributed to their agglomerated elongated TiO_2 nanowires in bulk form. On the other hand, both pure RGO and TiO_2NWs/RGO hybrid samples had large surface areas which is 103.61 m^2/g and 102.05 m^2/g, respectively. The samples display a similar pattern which is type IV having a hysteresis loop at relative pressure between 0.6 and 1, indicating pore size distributions in the mesoporous region (2 to 50 nm) as shown in Figure 4. Meanwhile, the hysteresis observed in the isotherms plot is matched with the H_3 type characteristic for the slit-shaped pores. A large specific surface area could provide more surface-active sites and facilitate the migration of charge carriers, which is useful to improve the photocatalytic performance, this benefits the photodegradation efficiency (Norouzi *et al.,* 2021). Somehow, the surface area of the TiO_2NWs/RGO hybrid sample is slightly lower as compared to pure RGO due to the presence of TiO_2NWs into/onto layered RGO which will block their pores (Prasad *et al.,* 2020). A similar pattern was obtained for the pore volume of the samples as RGO displays the highest values with 0.574 cm^3/g followed by TiO_2NWs/RGO hybrid and pristine TiO_2NWs samples which are 0.490 cm^3/g, and 0.233 cm^3/g, respectively.

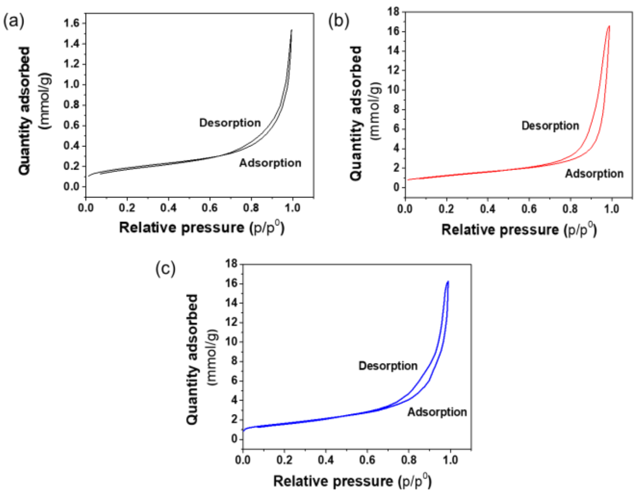

Figure 5. N2 adsorption-desorption isotherms of (a) TiO_2NWs, (b) RGO and (c) TiO_2NWs/RGO

E. Photocatalytic Activity

Figure 6 shows the photocatalytic activity of pristine TiO_2NWs, RGO and TiO_2NWs/RGO hybrid samples were investigated for methyl orange (MO) degradation under dark conditions and UV light. After 30 minutes, in dark condition the removal of MO was found to be 11%, 19%, 33% for TiO_2NWs, RGO and TiO_2NWs/RGO, respectively. Highest removal of MO using hybrid sample because of the synergy effect from TiO_2NWs and RGO. RGO has excellent in the mobility of charge carrier bring out fast absorption (Singh *et al.,* 2020) while elongated TiO_2 nanowires support further on adsorption of MO onto the hybrid sample. Moreover, the adsorption capacity of RGO has reached the maximum level after 2 hours. However, pure TiO_2NWs cannot fully degrade MO even after 3.5 hours of reaction due to their limited active site and fast electron and hole recombination in Figure 5. Figure 6 below shows the photodegradation reactions which take place on the surface of photocatalyst.

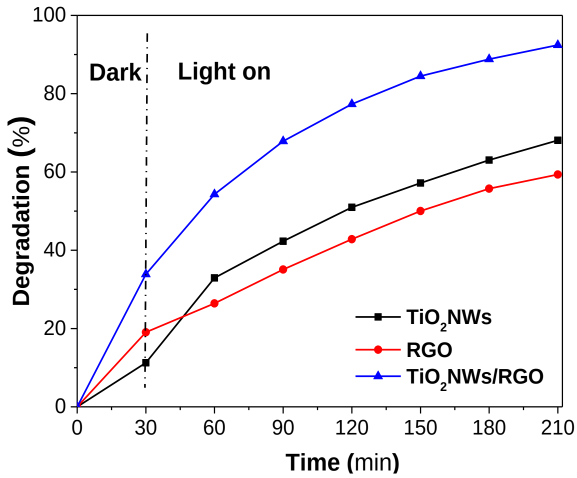

Figure 6. Percentage degradation of TiO_2NWs, RGO and TiO_2NWs/RGO within 210 minutes

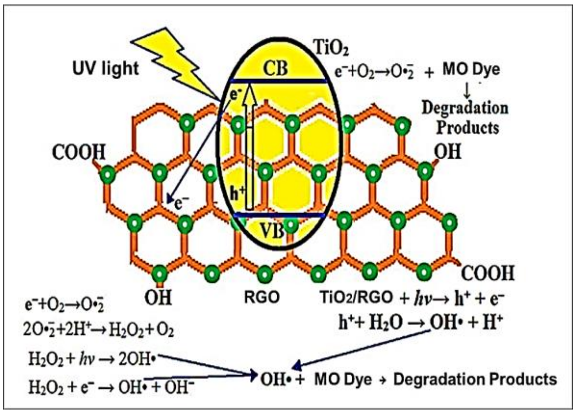

Figure 7. Photodegradation reaction of MO dye by using hybrid photocatalyst

Interestingly, in this study, the TiO_2NWs/RGO hybrid photocatalyst sample gave the highest degradation rate of MO with 92% at 210 minutes reaction. These results could be correlated to the enlargement of the active sites accessible to the pollutant molecules. Therefore, the combination of TiO_2NWs with other high surface materials could enhance their photocatalytic activity. However, Table 1 compiles the results found in the literature for MO dye degradation with different photocatalysts for comparison with the TiO_2NWs/RGO hybrid catalyst presented here, which showed increased photocatalytic activity.

Table 1. Summary of recent research reports on methyl orange degradation activity

Photocatalyst	**Mo Dye**	**Efficiency (%)**	**References**
TiO_2NWS/RGO (0.1 g)	20 ppm (100 ml)	92% after 210 min under UV light	This study
$CoFe_2O_4$-Ag_2O (3 g)	20 ppm (200 ml)	85% after 240 min under UV light	Sun *et al.*, 2020
Cu-doped ZnO (0.1g)	20 ppm (100 ml)	88% after 240 min under UV light	Fu *et al.*, 2011
$SnSO_4$-TiO_2 (0.3g)	20 ppm (75 ml)	91.3% after 14 hours under visible light	Yao *et al.*, 2021
TiO_2/ZnO/rGO (0.5g)	20 ppm (1L)	44.2% after 180 min under UV light	Hieu *et al.*, 2019
Ag/TiO_2 (0.1 g)	30 ppm (100 ml)	35% after 120 min under UV light	Zheng *et al.*, 2019

In a typical heterogeneous photocatalytic process, when an equilibrium adsorption process of the oxidant and the reductant species occurs based on the Langmuir type of adsorption, the adsorption extent of these materials plays a highly important role in the rate of the photodegradation process (Nourouzi *et al.,* 2021). Thus, the Langmuir-Hinshelwood (L-H) model has been widely used for studying the kinetic futures of heterogeneous photocatalysis processes. Generally, the presence of both the oxidant and the reductant in a monolayer at the solid-liquid interface is known as the controlling factor for the rate-determining step of the reaction (Sajjad *et al.,* 2010). Considering that the solid catalyst is present in a heterogeneous solid phase in the heterogeneous photocatalysis process and its amount is also important in the photodegradation rate, the process is considered as an apparent first-order equation (Sajjad *et al.,* 2010).

However, reaction kinetics is studied in this research to estimate the order of photocatalytic degradation reaction and the adsorption capacity of the different materials. Hybrid TiO_2NWs/RGO has a percentage dye removal efficiency of 92.42%. Figure 7 shows the correlation coefficient for the pseudo-first-order kinetic model is good for heterogeneous catalyst. Photocatalytic activity occurs as a result of the interaction of photocatalyst and UV irradiation that yields highly reactive hydroxyl radicals, which are believed to be the main species responsible for oxidation (Sakka, 2013). It has been found that for degradation of MO dye each sample obeys first-order reaction kinetics. It was fixed to the Langmuir–Hinshelwood model by plotting ln (C_o/C_t) against the irradiation time (t) to obtain straight lines with linear regression coefficients (R^2). Where C_o and C_t (both in mgL^{-1}) are the initial and remaining concentration of MO in solution, respectively, and C_t is the absorbance at any irradiation time. The pseudo-first-order rate constants, k (min^{-1}) for every photocatalyst were calculated from the slopes of the plots and are presented in Table 2. This study confirms that TiO_2NWS/RGO is responsible for the rapid degradation of MO dye.

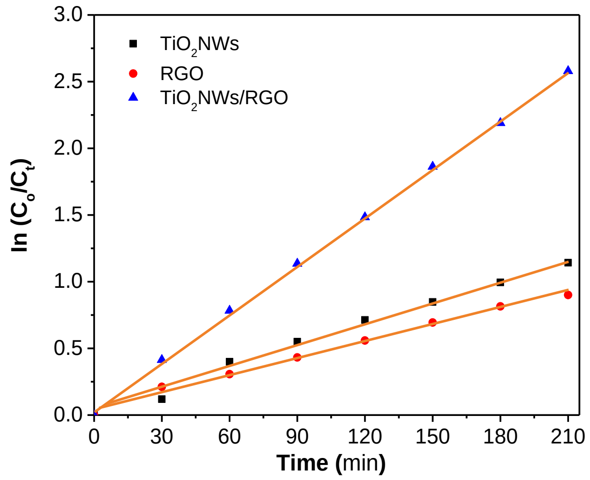

Figure 8. Kinetics of MO photodegradation according to the pseudo-first order equation

Table 2. The rate constant and Linear regression of kinetic

Photocatalyst	Rate constant (min^{-1})	Linear Regression(R^2)
TiO_2NWs	0.0055	0.9907
RGO	0.0042	0.9924
TiO_2NWs/RGO	0.0121	0.9995

IV. CONCLUSION

The TiO_2NWs/RGO nanocomposite was made using a fabrication method. FTIR analysis shows the presence of functional group of TiO_2NWs, RGO and XRD pattern confirmed the existence of both materials. Agglomerated TiO_2 nanowires (1D) and a layered structure (2D) of RGO were shown by SEM micrographs. The large surface area of the hybrid increases the photocatalytic efficiency of methyl orange dye degradation. The successful separation of photogenerated carriers and the wide optical absorption, both owing to the interaction developed between TiO_2NWs/RGO contributed to the photocatalytic efficiency capability.

V. ACKNOWLEDGEMENT

The authors are grateful to Universiti Malaysia Terengganu (UMT) for facilities and Malaysia Ministry of Higher Education for the financial support vote (FRGS/1/2019/STG07/UMT/02/2).

VI. REFERENCES

Alshammari, AS, Halim, MM, Yam, FK & Kaus NHM 2020, 'Synthesis of Titanium Dioxide (TiO_2)/Reduced Graphene Oxide (rGO) thin film composite by spray pyrolysis technique and its physical properties', Material Science in Semiconducting processing, vol. 116, pp. 105-140.

Akyuz, D, Keskin, B, Sahinturk, U & Koca, A 2016, 'Electrocatalytic hydrogen evolution reaction on reduced graphene oxide electrode decorated with cobaltphthalocyanine', Applied Catalysis B: Environmental, vol. 188, pp. 217-226

Barnard, AS & Curtiss, LA 2005, 'Prediction of TiO2 nanoparticle phase and shape transitions controlled by surface chemistry', Nano Letters, vol. 5, pp. 1261–1266.

Bashiri, F, Khezri, SM, Kalantary, RR & Kakavandi, B 2020, 'Enhanced photocatalytic degradation of metronidazole by TiO_2 decorated on magnetic reduced graphene oxide: Characterization, optimization and reaction mechanism studies', Journal of Moleculars Liquids, vol. 314, pp. 113-608.

Boruah, PK & Das, MR 2019, 'Dual responsive magnetic Fe3O4-TiO2/graphene nanocomposite as an artificial nanozymes for the colorimetric detection and photodegradation of pesticide in an aqueous medium', Journal of Hazardous Materials, pp. 121516.

Fu, M, Li, Y, wu, S, Lu, P, Liu, J & Dong, F 2011, 'Sol–gel preparation and enhanced photocatalytic performance of Cu-doped ZnO nanoparticles', Applied Surface Science, vol. 258, no. 4, pp. 1587–1591.

Gao, Z, Liu, N, Wu, D, Tao, W, Xu, F & Jiang, K 2012, 'Graphene–CdS composite, synthesis and enhanced photocatalytic activity', Applied Surface Science, vol. 258, pp. 2473-247.

Geng, NN, Chen, W, Xu, H, Lin, T, Ding, MM, Wang, Y, Tao, H & Hu, K 2019, 'Preparation of Fe3O4/TiO2-N-GO sonocatalyst and using for humic acid removal with the assist of ultrasound', Materials Science in Semiconductor Processing, vol. 102, pp. 104593.

Gonçalves, BS, Palhares, HG, Souza, TCD, Castro, VGD, Silva, GG, Silva, BC & Nunes, EH 2019, 'Effect of the carbon loading on the structural and photocatalytic properties of reduced graphene oxide-TiO_2 nanocomposites prepared by hydrothermal synthesis', Journal of Materials Research and Technology, vol. 8, no. 6, pp. 6262-6274.

Hatefi, R, Younesi, H, Mashinchian-Moradi, A & Nojavan, S 2021, 'A facile decoration of anatase Fe_3O_4/TiO_2 nanocomposite with graphene quantum dots: Synthesis, characterization, and photocatalytic activity', Advanced Powder Technology.

Hieu NC, Lien TM, Tuong VTT & Juang, R-S, 2019, 'Enhanced removal of various dyes from aqueous solutions by UV and simulated solar photocatalysis over TiO2/ZnO/rGO composites', Separation and Purification Technology, pp. 115962.

Ikram, M, Ali, S, Aqeel,M, UI-Hamid, A, Imran, M, Haider, J, Shahbaz, A & Ali, S, 2020, 'Reduced graphene oxide nanosheets doped by Cu with highly efficient visible light photocatalytic behaviour', Journal of Alloys and compound, vol. 837. pp. 155-588.

Kamalam, MBR, Inbanathan, S & Sethuraman, K, 2018, 'Enhanced photo catalytic activity of graphene oxide/MoO_3 nanocomposites in the degradation of Victoria Blue Dye under visible light irradiation', Applied Surface Science, vol. 449, pp. 685-695.

Khan, SA, Arshad, Z, Shahid, S, Arshad, I, Rizwan, K, Sher, M & Fatima, U 2019, 'Synthesis of TiO_2/graphene oxide nanocomposites for their enhanced photocatalytic activity against methylene blue dye and ciprofloxacin', Composites Part B: Engineering, vol. 175, pp. 107-120.

Kumar, SG & Devi, LG 2011, 'Review on modified TiO2Photocatalysis under UV/visible light: selected results and related mechanisms on interfacial charge carrier transfer dynamics', The Journal of Physical Chemistry A, vol. 115, no. 46, pp. 13211–13241.

Li, X, Shen, R, Ma, S, Chen, X & Xie, J 2018 'Graphene-based heterojunction photocatalysts', Applied Surface Science, vol. 430, pp. 53-107.

Liu, B & Zeng, HC, 2008, 'Carbon nanotubes supported mesoporous mesocrystals of anatase TiO_2', Chemistry of Materials, vol. 20, no. 8, pp. 2711–2718.

Madadrang, CJ, Kim, HY, Gao, G, Wang, N, Zhu, J, Feng, H, Gorring, M, Kasner, ML & Hou, S 2012, 'Adsorption behavior of EDTA-graphene oxide for PB (ii) removal', ACS Applied Materials & Interfaces, vol. 4, no. 3, pp. 1186–1193.

Makal, P & Das, D 2019, 'Superior photocatalytic dye degradation under visible light by reduced graphene oxide laminated TiO_2-B nanowire composite', Journal of Environmental Chemical Engineering, vol. 9, no. 5, pp. 103-358.

Marien, CBD, Cottineau, T, Robert, D & Drogui, P 2016, 'TiO_2 Nanotube arrays: Influence of tube length on the photocatalytic degradation of Paraquat', Applied Catalyst B: Environment, vol. 194, pp. 1-6.

Maruthamani, D, Divakar, D & Kumarave, M, 2015, 'Enhanced photocatalytic activity of TiO_2 by reduced graphene oxide in mineralization of Rhodamine B dye', Journal of Industrial and Engineering Chemistry, vol. 30, pp. 33-43.

Najafi, M, Kermanpur, A, Rahimipour, MR & Najafizadeh, A, 2017, 'Effect of TiO_2 morphology on structure of TiO_2-graphene oxide nanocomposite synthesized via a one-step hydrothermal method', Journal of Alloys and Compounds, vol. 722, pp. 272-277.

Norouzi, A, Nezamzadeh-Ejhieh, Alireza & Fazaeli, R 2021, 'A Copper(I) oxide-zinc oxide nano-catalyst hybrid: Brief characterization and study of the kinetic of its photodegradation and photomineralization activities toward methylene blue', Materials Science in Semiconductor Processing, vol. 122, pp. 105495.

Piler, K, Bahrim, C, Twagirayezu, S & Benson, TJ, 2020, 'Lattice disorders of tio2 and their significance in the photocatalytic conversion of CO2', Advances in Catalysis, pp. 109–233.

Prasad, C, Liu, Q, Tang, H, Yuvaraja, G, Long, J, Rammohan, A & Zyryanov, GV 2020, 'An overview of graphene oxide supported semiconductors based photocatalysts: Properties, synthesis and photocatalytic applications', Journal of Molecular Liquids, vol. 297, pp. 111-826.

Putri LK, Ong WJ, Chang WS & Chai SP 2016, 'Graphene oxide: Exploiting its unique properties toward visible-light-driven photocatalysis', Applied Materials today, pp. 49-16.

Sajjad, AKL, Shamaila, S, Tian, B, Chen, F & Zhang, J 2010, 'Comparative studies of operational parameters of degradation of azo dyes in visible light by highly efficient WOx/TiO2 photocatalyst', Journal of Hazardous Material, vol. 177, pp. 781–791.

Sakka, S 2013, Handbook of Advanced Ceramics, Sol–Gel Process and Applications, pp. 883–910.

Singh, P, Shandilya, P, Raizada, P, Sudhaik, A, Rahmani-Sani, A & Hosseini-Bandegharaei, A 2020, 'Review on various strategies for enhancing photocatalytic activity of graphene based nanocomposites for water purification', Arabian Journal of Chemistry, vol. 13, no. 1, pp. 3498-3520.

Schneider, J, Matsuoka, M, Takeuchi, M, Zhang, J, Horiuchi, Y, Anpo, M & Bahnemann, DW 2014, 'Understanding TiO2 photocatalysis: mechanisms and materials', Chemical Reviews, vol. 114, no. 19, pp. 9919–9986.

Shymanovska, VV, Khalyavka, TA, Manuilov, EV, Gavrilko, TA, Aho, A, Naumov, VV & Shcherban, ND 2022, 'Effect of surface doping of TIO_2 powders with Fe ions on the structural, optical and photocatalytic properties of anatase and rutile', Journal of Physics and Chemistry of Solids, vol. 160, pp. 110-308.

Sun, F, He, J, Wu, P, Zeng, Q, Liu, C & Jiang, W 2020, 'Magnetic photocatalyst $CoFe_2O_4$-Ag_2O with magnetic aggregation bed photocatalytic reactor for continuous photodegradation of methyl orange', Chemical Engineering Journal, pp. 125-397.

Wei, X, Ou, C, Guan, X, Peng, Z & Zheng, X 2019, 'Facile assembly of CdS-reduced graphene oxide heterojunction with enhanced elimination performance for organic pollutants in wastewater', Applied Surface Science, vol. 469, pp. 666-673.

Xie, H, Ye, X, Duan, K, Xue, M, Du, Y, Ye, W & Wang, C 2015, 'CuAu–ZnO–graphene nanocomposite: A novel graphene-based bimetallic alloy-semiconductor catalyst with its enhanced photocatalytic degradation performance', Journal of Alloys and Compounds, vol. 636, pp. 40-47.

Yao, X, Zhang, B, Cui, S, Yang, S & Tang, X 2021, 'Fabrication of $SnSO_4$-modified TiO_2 for enhance degradation performance of methyl orange (MO) and antibacterial activity', Applied Surface Science, vol. 551, pp. 149419.

Zhao, X, Li, Y, Wang, J, Ouyang, Z, Li, J, Wei, G & Su, Z 2014, 'Interactive oxidation–reduction reaction for the in situ synthesis of graphene–phenol formaldehyde composites with enhanced properties', ACS Applied Materials and Interfaces, vol. 6, no. 6, pp. 4254–4263.

Zheng, X, Zhang, D, Gao, Y, Wu, Y, Liu, Q & Zhu, X 2019, 'Synthesis and characterization of cubic Ag/TiO_2 nanocomposites for the photocatalytic degradation of methyl orange in aqueous solutions', Inorganic Chemistry Communications, vol. 110, pp. 107589.